CHIN. PHYS. LETT. Vol. 35, No. 4 (2018) 043202

Kramers–Henneberger Form of Strong Field Theory with the Correction of Dipole Approximation *

Yi-Ning Huo(霍一宁)[1], Jian Li(李健)[2,3], Feng-Cai Ma(马凤才)[1,3]**

[1]*School of Physics, Liaoning University, Shenyang 110036*
[2]*School of Physical Science and Technology, Inner Mongolia University, Hohhot 010021*
[3]*Department of Science, Shenyang Aerospace University, Shenyang 110036*

(Received 22 August 2017)

We show that the breakdown of dipole approximation can be adopted to explain the asymmetry structure in the photoelectron momentum distributions along the beam propagation direction, which is defined as the photoelectron longitudinal momentum distributions (PLMD), in tunneling regime ($\gamma_{\rm K} \ll 1$), based on the strong field approximation theory. The nondipole Hamiltonian for photoelectrons interacting with laser fields from a hydrogen-like atom is transformed into the Kramers–Henneberger frame in our model. To introduce the correction of dipole approximation, the spatial variable is kept in a vector potential $\boldsymbol{A}(\boldsymbol{r},t)$, demonstrating that the breakdown of dipole approximation is the major reason for the shift of the peak in PLMD. The nondipole effects are apparent when circularly polarized lasers are adopted to ionize the atoms, and clear tendency to increase offsets is found for increasing laser intensities.

PACS: 32.80.Fb DOI: 10.1088/0256-307X/35/4/043202

Over the past several decades, the strong field approximation (SFA) theory[1–3] has provided us with an insightful method to understand the photoionization processes of atoms and molecules caused by a strong laser field. A series of studies involving experiments and theories have recently been reported, stimulating us to reconsider the nature of a photoelectron in a strong laser field because the longitudinal velocity of the photoelectron has been regarded to exert profound effects on the photoionization.[4,5] The photoelectron longitudinal momentum distributions (PLMD) were initially believed to show a Gaussian structure.[6–9] However, Arissian *et al.*[10] and Smeenk *et al.*[11] reported that a small positive shift is observed in the center from zero in the PLMD when neon or argon was ionized by a circularly polarized laser. This characteristic asymmetry was analyzed in detail by Titi and Drake[12] and Reiss.[13] Ludwig *et al.*[14] reported a different phenomenon involving an increasing shift of the peak of the PLMD in the direction opposite to the beam propagation direction, which was totally divergent from that observed in previous investigations. The semi-classical re-scattering process[15] was introduced to explain the distinct phenomenon and to investigate the PLMD produced by a linearly polarized laser. Chelkowski *et al.*[16] revealed that PLMD exhibits a positive shift when the Lorentz force is considered. Meanwhile, the photoelectron released from the hydrogen-like atom associated with the re-scattering process, which involves the parent ion, revealed a negative shift in the PLMD. The difference in the photoelectron energy spectra between the direct and re-scattered ionization was recently investigated.[17,18] These studies inspire us to establish a new approach, based on the SFA theory to investigate the PLMD in the direct ionization caused by the linearly polarized laser or the ionization caused by the circularly polarized laser.

One of the most significant approximations is the dipole approximation in SFA. Any spatial dependence of the applied field and the homogeneous magnetic field component can be ignored in the Hamiltonian. Commonly, the atom size is very small compared with the wavelength of the laser. Therefore, we can adopt the approximation to calculate and analyze the interactions between the atoms and the applied laser. However, the breakdown of the dipole approximation accounts for the asymmetry due to the Lorentz force component.[16] The validity of the dipole approximation obviously decreases when a high-intensity or low-frequency laser is employed.[19–21] Therefore, we analyze whether the asymmetric structure in the tunnel regime $\gamma_{\rm K} \ll 1$[1] ($\gamma_{\rm K}$ is the Keldysh parameter) can be explained. The spatial dependence is retained in the vector potential to reflect the nondipole effects. A useful approximation is used to decrease the influence of the Coulomb potential in our model by combining Green's function, considering that the laser intensity is enormous in the tunnel regime, referring to the high-intensity long-wavelength limit.

The Kramers–Henneberger (KH) frame[22] is applied to study the issue in the high-intensity low-frequency regime, where the component of the magnetic field becomes important enough, and the nondipole effects are apparent because the laser intensity I (expressed in atomic units) is enormous. The vector potential is $\boldsymbol{A}(\eta) = a\boldsymbol{\varepsilon}\cos(\eta)$ with $\eta = \omega t - \boldsymbol{k}\cdot\boldsymbol{r}$, where $\boldsymbol{k}$ is the propagation vector, ω stands for the frequency, and a stands for the amplitude. The atomic units (a.u.) $m = e = \hbar = 1$ and $c = 137$ are utilized throughout this study unless indicated otherwise. Thus the Schrödinger equation is presented as

$$i\partial_t|\psi_{\rm f}(\boldsymbol{r},t)\rangle = \Big[\frac{1}{2}\Big(\boldsymbol{p} + \frac{\boldsymbol{A}(\eta)}{c}\Big)^2 + V(\boldsymbol{r})\Big]|\psi_{\rm f}(\boldsymbol{r},t)\rangle. \quad (1)$$

*Supported by the National Natural Science Foundation of China under Grant Nos 11274149 and 11304185, and the Program of Shenyang Key Laboratory of Optoelectronic Materials and Technology under Grant No F12-254-1-00.
**Corresponding author. Email: fcma@lnu.edu.cn
© 2018 Chinese Physical Society and IOP Publishing Ltd

A new wave function can be introduced according to Henneberger's study,[22]

$$|\psi_{\rm KH}(\boldsymbol{r},t)\rangle = \hat{U}_{\rm KH}(\boldsymbol{r},t)|\psi_{\rm f}(\boldsymbol{r},t)\rangle, \tag{2}$$

where $\hat{U}_{\rm KH}(\boldsymbol{r},t) = \hat{U}_{\rm KH2}(\boldsymbol{r},t)\hat{U}_{\rm KH1}(\boldsymbol{r},t)$, $\hat{U}_{\rm KH2}(\boldsymbol{r},t) = e^{[\frac{i}{\omega}\int_{\eta_{\rm i}}^{\eta_{\rm f}} d\eta \frac{\boldsymbol{A}(\eta)\cdot\boldsymbol{p}}{c}]}$, and $\hat{U}_{\rm KH1}(\boldsymbol{r},t) = e^{[\frac{i}{\omega}\int_{\eta_{\rm i}}^{\eta_{\rm f}} d\eta \frac{\boldsymbol{A}(\eta)^2}{2c^2}]}$. Under the KH frame, Eq. (1) can be transformed to

$$i\partial_t|\psi_{\rm KH}(\boldsymbol{r},t)\rangle = \hat{H}_{\rm KH}|\psi_{\rm KH}(\boldsymbol{r},t)\rangle, \tag{3}$$

where $\hat{H}_{\rm KH}$ is given by $\hat{H}_{\rm KH} = \frac{\boldsymbol{p}^2}{2} + V(\boldsymbol{r}+\boldsymbol{\alpha}(\eta))$ and $\boldsymbol{\alpha} = \frac{1}{c\omega}\int_{\eta_{\rm i}}^{\eta_{\rm f}} \boldsymbol{A}(\eta)d\eta$. Using Green's function, $G(t,t') = -i\theta(t-t')\int d\boldsymbol{p}|\varphi(\boldsymbol{p},t)\rangle\langle\varphi(\boldsymbol{p},t)|$, the solution of Eq. (3) can be obtained as

$$|\psi_{\rm KH}(\boldsymbol{r},t)\rangle = |\psi(\boldsymbol{r},t)\rangle + \int G(t,t')\cdot V(\boldsymbol{r} + \boldsymbol{\alpha}(\eta))|\psi_{\rm KH}(\boldsymbol{r},t')\rangle dt', \tag{4}$$

where $|\psi(\boldsymbol{r},t)\rangle$ is the plane wave function given by $|\psi(\boldsymbol{r},t)\rangle = \frac{1}{\sqrt[3]{2\pi}}\exp[i(\boldsymbol{p}\cdot\boldsymbol{r} - \omega t)]$. Based on Eq. (4), we can resolve Eq. (1) as $|\psi_{\rm f}(\boldsymbol{r},t)\rangle = \hat{U}_{\rm KH}^{-1}(\boldsymbol{r},t)|\psi_{\rm KH}(\boldsymbol{r},t)\rangle$. The final state of the ejected photoelectron in the S-matrix is $|\psi_{\rm f}(\boldsymbol{r},t)\rangle$, instead of the Volkov state,[23,24] and $\hat{H}_{\rm I}$ is used to describe the interaction with the laser field in the velocity gauge.[2] The S-matrix expression can be written as

$$(S-1)_{\rm fi} = -i\int_{-\infty}^{\infty} dt\langle\psi_{\rm f}(\boldsymbol{r},t)|\hat{H}_{\rm I}(\eta)|\phi_{\rm i}(\boldsymbol{r},t)\rangle, \tag{5}$$

where $\hat{H}_{\rm I} = \frac{1}{c}\boldsymbol{A}(\eta)\cdot\boldsymbol{p} + \frac{1}{2c^2}\boldsymbol{A}(\eta)^2$, and $|\phi_{\rm i}(\boldsymbol{r},t)\rangle$ is the bound state. Using $|\psi_{\rm f}(\boldsymbol{r},t)\rangle$, Eq. (5) can be expressed as

$$\begin{aligned}(S-1)_{\rm fi} = &-i\int_{-\infty}^{\infty} dt\langle\varphi(\boldsymbol{r},t)|\hat{H}_{\rm I}(\eta)|\phi_{\rm i}(\boldsymbol{r},t)\rangle\\ &-i\int_{-\infty}^{\infty} dt\langle\int dt' G(t,t')\cdot V(\boldsymbol{r}\\ &+\boldsymbol{\alpha}(\eta))\varphi(\boldsymbol{r},t)|\hat{H}_{\rm I}(\eta)|\phi_{\rm i}(\boldsymbol{r},t)\rangle\\ &-i\int_{-\infty}^{\infty} dt\langle\int dt' G(t,t')\cdot V(\boldsymbol{r}\\ &+\boldsymbol{\alpha}(\eta))\cdot G(t',t'')V(\boldsymbol{r}\\ &+\boldsymbol{\alpha}(\eta))\varphi(\boldsymbol{r},t)|\hat{H}_{\rm I}(\eta)|\phi_{\rm i}(\boldsymbol{r},t)\rangle\\ &-i\int_{-\infty}^{\infty} dt\langle\int dt' G(t,t')\cdot V(\boldsymbol{r}\\ &+\boldsymbol{\alpha}(\eta))\cdot G(t',t'')V(\boldsymbol{r}+\boldsymbol{\alpha}(\eta))\ldots\varphi(\boldsymbol{r},t)\\ &\cdot|\hat{H}_{\rm I}(\eta)|\phi_{\rm i}(\boldsymbol{r},t)\rangle.\end{aligned} \tag{6}$$

The first and second terms could be retained to calculate the S-matrix in the tunneling ionization when a laser with a high intensity and low frequency is used. The vector potential is $\boldsymbol{A} = \boldsymbol{\varepsilon}a\cos(\omega t - \boldsymbol{k}\cdot\boldsymbol{r}) = \boldsymbol{\varepsilon}a\cos\eta$, and the Coulomb potential can be transformed to $V_{\rm l}(\boldsymbol{r}+\boldsymbol{\alpha}) = \frac{-1}{|\boldsymbol{r}+(a\boldsymbol{\varepsilon}/c\omega)\sin(\eta)|}$ when a linearly polarized laser is applied. The directly ionized photoelectron produced by the high-intensity linearly polarized laser is also analyzed. The value of $|\boldsymbol{\alpha}(t)| = \frac{\sqrt{I}}{\omega^2} = \frac{F}{\omega^2}$ is the radius of the quiver motion of photoelectrons exposed to laser fields, where F is the electric field vector amplified for the linear ($I = F^2$) and circular ($I = 2F^2$) polarizations. The laser fields with a high-intensity long-wavelength limit are analyzed, and it is accepted that $|\boldsymbol{\alpha}(t)| \gg a_0/Z$,[25,26] with a_0 being the Bohr radius. Hence it is valid to assume $|\boldsymbol{r}| \ll |\boldsymbol{\alpha}(t)|$ in the tunnel regime.

Using $V_{\rm l}(\boldsymbol{r}+\boldsymbol{\alpha}) = \frac{-1}{|\boldsymbol{r}+(a\boldsymbol{\varepsilon}/c\omega)\sin(\eta)|} \cong \frac{-1}{|(a\boldsymbol{\varepsilon}/c\omega)\sin(\eta)|}$, we can obtain

$$\begin{aligned}&\int_{-\infty}^{t} dt' G(t,t')V_{\rm l}(\tau)|\varphi_{\rm i}(\boldsymbol{r},t')\rangle\\ &\quad= \frac{i}{(2\pi)^{3/2}}\cdot\frac{e^{(i\boldsymbol{p}\cdot\boldsymbol{r})}}{\sqrt{I}/\omega^2}\cdot\int_{-\infty}^{t}\frac{e^{(-iEt')}}{\sin(\omega t')}dt'.\end{aligned} \tag{7}$$

Expanding $\frac{1}{\sin(\omega t')}$ around $\omega t'$, using $\frac{1}{\sin(\omega t')} = 2i\cdot e^{(-i\omega t')}\cdot\sum_{n=0}^{\infty} e^{(-2in\omega t')}$, and maintaining up to the linear order due to the infrared light, we obtain

$$\begin{aligned}|\psi_{\rm KH}^{\rm l}(\boldsymbol{r},t)\rangle &= |\varphi(\boldsymbol{r},t)\rangle + \int G(t,t')V_{\rm l}(\boldsymbol{r}+\boldsymbol{\alpha}(t'))|\varphi_k(\boldsymbol{r},t')\rangle dt'\\ &= |\varphi(\boldsymbol{r},t)\rangle + \frac{-2i}{(2\pi)^{3/2}}\frac{e^{(i\boldsymbol{p}\cdot\boldsymbol{r})}}{\sqrt{I}/\omega^2}\left(\frac{1}{E+\omega}\right)\cdot\Big\{-e^{[i(E+\omega)t]}\\ &\quad-\left(\frac{E+\omega}{E+3\omega}\right)\cdot e^{[i(E+3\omega)t]}\Big\}.\end{aligned} \tag{8}$$

Hence, the intensity amplitude $\zeta_{\rm l} = \frac{-a\boldsymbol{\varepsilon}\cdot\boldsymbol{p}}{\omega c}$ and the intensity parameter $z = \frac{a^2}{4\omega c^2} = \frac{U_{\rm p}}{\omega}$[2] are introduced, where $U_{\rm p}$ is the ponderomotive energy of the electron. The expression of $|\psi_{\rm f}^{\rm l}(\boldsymbol{r},t)\rangle$ can be rewritten as $|\psi_{\rm f}^{\rm l}(\boldsymbol{r},t)\rangle = (\hat{U}_{\rm KH}^{\rm l})^{-1}|\psi_{\rm KH}^{\rm l}(\boldsymbol{r},t)\rangle$, where the S-matrix can be divided into two parts as

$$(S-1)_{\rm fi}^{l} = (S-1)_{\rm fi}^{l\ (0)} + (S-1)_{\rm fi}^{l\ (1)}, \tag{9a}$$

$$\begin{aligned}(S-1)_{\rm fi}^{l\ (0)} = &-i\int_{-\infty}^{\infty} dt\frac{1}{(2\pi)^{3/2}}\\ &\cdot e^{[-i\boldsymbol{p}\cdot\boldsymbol{r}+iEt-i\zeta_{\rm l}\sin(\eta)+iz\cdot\frac{\sin(2\eta)}{2}+iz\eta]}\\ &\cdot[-\zeta_{\rm l}\omega\cos(\eta)+z\omega\cos(2\eta)+z\omega]\phi_{\rm i}(\boldsymbol{r})e^{-iE_{\rm i}t},\end{aligned} \tag{9b}$$

$$\begin{aligned}(S-1)_{\rm fi}^{l\ (1)} = &-i\int_{-\infty}^{\infty} dt\frac{1}{(2\pi)^{3/2}}\\ &\cdot e^{[-i\zeta_{\rm l}\sin(\eta)+iz\cdot\frac{\sin(2\eta)}{2}+iz\eta]}\\ &\times\frac{2i}{(2\pi)^{3/2}}\frac{e^{(-i\boldsymbol{p}\cdot\boldsymbol{r})}}{(\sqrt{I}/\omega^2)\cdot(E+\omega)}\Big\{-e^{[-i(E+\omega)t]}\\ &-e^{[-i(E+3\omega)t]}\left(\frac{E+\omega}{E+3\omega}\right)\Big\}\\ &\times[-\zeta_{\rm l}\omega\cos(\eta)+z\omega\cos(2\eta)+z\omega]\phi_{\rm i}(\boldsymbol{r})e^{(-iE_{\rm i}t)}.\end{aligned} \tag{9c}$$

When the nature of the general Bessel function is considered,[2] $\sum_{n=-\infty}^{\infty} e^{in\phi}J_n(u,v) = e^{i(u\sin\phi+v\sin 2\phi)}$. Introducing the momentum representation of the initial state of the hydrogen-like atom $\phi_{\rm i}(\boldsymbol{r}) =$

$\int d^3\boldsymbol{p}'\tilde{\phi}_{\rm i}(\boldsymbol{p}')e^{i\boldsymbol{p}'\cdot\boldsymbol{r}}$ by the Fourier transformation, $(S-1)_{fi}^{l\ (0)}$ can be obtained as

$$(S-1)_{\rm fi}^{l\ (0)} = -2\pi i\Big(z\omega A_0 - \frac{\zeta_{\rm l}\omega}{2}A_1 - \frac{\zeta_{\rm l}\omega}{2}A_{-1} + \frac{z\omega}{2}A_2 + \frac{z\omega}{2}A_{-2}\Big), \tag{10}$$

where $A_{\rm l} = \sum\limits_{n\geqslant n_0} J_n(\zeta_{\rm l}, -\frac{z}{2})\cdot\tilde{\phi}_{\rm i}(\boldsymbol{p}-(n+l-z)\boldsymbol{k})\cdot\delta(E+(z-n-l)\omega+E_{\rm b})$ with $E_{\rm b} = -E_{\rm i} = \frac{Z^2}{2n_{\rm l}^2}$ being the binding energy. We set the nuclear charge $Z=1$, corresponding to a hydrogen atom, $n_{\rm l}$ is the quantum number, and $n_0 = [z+E_{\rm b}/\omega]_{\rm int}+1$, which is treated as the minimal number of photons absorbed ($[\ldots]$ denotes the integer part of the expression). Combining with the important expression[27] related to the general Bessel function $2nJ_n(u,v) = u[J_{n-1}(u,v)+J_{n+1}(u,v)] + 2v[J_{n-2}(u,v)+J_{n+2}(u,v)]$, Eq. (10) can be simplified to

$$(S-1)_{\rm fi}^{l\ (0)} = -2\pi i\sum_{n\geqslant n_0}(z-n)J_n\Big(\zeta_{\rm l},-\frac{z}{2}\Big)\cdot\tilde{\phi}_{\rm i}(\boldsymbol{p}-(n-z)\boldsymbol{k})\delta(E+(z-n)\omega+E_{\rm b}). \tag{11}$$

Similarly, $(S-1)_{fi}^{l\ (1)}$ can be rewritten as

$$\begin{aligned}(S-1)_{fi}^{l\ (1)} =& \sum_{n\geqslant n_0-1}\Big(\frac{-4\pi}{\frac{\sqrt{I}}{\omega^2}(E+\omega)}\Big)\cdot(n-z)\omega\\ &\cdot J_n\Big(\zeta_{\rm l},\frac{-z}{2}\Big)\cdot\tilde{\phi}_{\rm i}(\boldsymbol{p}-(n-z)\boldsymbol{k})\\ &\cdot\delta((E+\omega)+(z-n)\omega+E_{\rm b})\\ &+\sum_{n\geqslant n_0-3}\Big(\frac{-4\pi}{\frac{\sqrt{I}}{\omega^2}(E+\omega)}\Big)\cdot(n-z)\omega\\ &\cdot J_n\Big(\zeta_{\rm l},\frac{-z}{2}\Big)\cdot\tilde{\phi}_{\rm i}(\boldsymbol{p}-(n-z)\boldsymbol{k})\\ &\cdot\Big(\frac{\omega+E}{3\omega+E}\Big)\cdot\delta((E+3\omega)+(z-n)\omega+E_{\rm b}).\end{aligned} \tag{12}$$

Altering n in the second term on the right side, Eq. (12) can then be simplified to

$$\begin{aligned}(S-1)_{\rm fi}^{l\ (1)} =& \sum_{n\geqslant n_0-1}\Big(\frac{-4\pi}{(\sqrt{I}/\omega^2)\cdot(E+\omega)}\Big)\\ &\cdot\delta((E+\omega)+(z-n)\omega+E_{\rm b})\Big\{(n-z)\omega\cdot J_n(\zeta_{\rm l},\frac{-z}{2})\\ &\cdot\tilde{\phi}_{\rm i}(\boldsymbol{p}-(n-z)\boldsymbol{k})+(n-2-z)\omega\\ &\cdot J_{n-2}(\zeta_{\rm l},\frac{-z}{2})\cdot\tilde{\phi}_{\rm i}(\boldsymbol{p}-(n-2-z)\boldsymbol{k})\Big(\frac{\omega+E}{3\omega+E}\Big)\Big\}.\end{aligned} \tag{13}$$

The applied vector potential can be expressed as $\boldsymbol{A} = \frac{a}{\sqrt{2}}(\boldsymbol{e}_x\cos(\eta)\pm\boldsymbol{e}_y\sin(\eta))$ when a circularly polarized laser is used. The electromagnetic wave propagation is in the direction of the z-axis, and $\boldsymbol{e}_x$, $\boldsymbol{e}_y$ are the unit vectors along the x and y axes, respectively. Similar to the linearly polarized ionization, $V_{\rm c}(\boldsymbol{r}+\boldsymbol{\alpha}) \cong \frac{-1}{\sqrt{I/2\cdot(1/\omega^2)}}$, when the laser intensity is large enough. The S-matrix is now presented as

$$(S-1)_{\rm fi}^{c} = (S-1)_{\rm fi}^{c\ (0)} + (S-1)_{\rm fi}^{c\ (1)}, \tag{14}$$

$$(S-1)_{\rm fi}^{c\ (0)} = -2\pi i\sum_{n\geqslant n_0}J_n(\zeta_{\rm c})\cdot(z-n)\omega\tilde{\phi}_{\rm i}(\boldsymbol{p}-(n-z)\boldsymbol{k})\cdot\delta(E+(z-n)\omega+E_B)\cdot\exp(\mp i\vartheta), \tag{15}$$

$$(S-1)_{\rm fi}^{c\ (1)} = \frac{2\pi i}{\sqrt{\frac{I}{2}\cdot\frac{E}{\omega^2}}}\sum_{n\geqslant n_0}J_n(\zeta_{\rm c})\cdot(z-n)\omega\tilde{\phi}_{\rm i}(\boldsymbol{p}-(n-z)\boldsymbol{k})\cdot\delta(E+(z-n)\omega+E_{\rm b})\cdot\exp(\mp i\vartheta), \tag{16}$$

where $\vartheta = \arctan(p_y/p_x)$ is the phase angle derived from the definition[2] $\boldsymbol{\varepsilon}\cdot\boldsymbol{p} = |\boldsymbol{\varepsilon}\cdot\boldsymbol{p}|e^{\mp i\vartheta}$.

The initial states of the hydrogen-like atom are taken into account, and θ is defined as the polar angle between $\boldsymbol{r}$ and the polarization direction

$$\tilde{\phi}_{1S} = \frac{1}{\pi}\sqrt{8Z^5}\frac{1}{[Z^2+p^2]^2}, \tag{17}$$

$$\tilde{\phi}_{21-1}(\boldsymbol{p}) = \frac{-i\cdot(Z/2)^{7/2}}{\sqrt{2}\pi}\frac{p\sin\theta e^{-i\varphi}}{[(Z/2)^2+p^2]^3}, \tag{18}$$

$$\tilde{\phi}_{211}(\boldsymbol{p}) = \frac{i\cdot(Z/2)^{7/2}}{\sqrt{2}\pi}\frac{p\sin\theta e^{-i\varphi}}{[(Z/2)^2+p^2]^3}. \tag{19}$$

The total probability W in the cylindrical coordinate is presented as

$$W = \int wp_\perp dp_\perp dp_z d\varphi, \tag{20}$$

where $p_\perp = \sqrt{p^2-p_z^2}$ denotes the photoelectron momentum in the polarization plane, and azimuth φ is the angle between the direction of the polarization vector and the direction of $p_\perp$.

When the photoelectron is released from a ground state of the hydrogen-like atom, the ionization rate per unit of longitudinal momentum at a certain intensity is obtained as

$$\begin{aligned}\frac{dW_{\rm l}}{dp_z} =& \int d\varphi\sum_{n\geqslant n_0}\frac{32(n-z)^2\omega^2Z^5p_\perp|J_n(\zeta_{\rm l},\frac{-z}{2})|^2}{[Z^2+((n-z)\boldsymbol{k}-\boldsymbol{p})^2]^4}\\ &+\sum_{n\geqslant n_0-1}\frac{128(n-z)^2\omega^2Z^5}{(\frac{\sqrt{I}}{\omega^2})^2\cdot(E+\omega)^2}\frac{|J_n(\zeta_{\rm l},\frac{-z}{2})|^2p_\perp}{[Z^2+((n-z)\boldsymbol{k}-\boldsymbol{p})^2]^4}\\ &+\sum_{n\geqslant n_0-1}\frac{256(n-z)^2\omega^2Z^5}{(\frac{\sqrt{I}}{\omega^2})^2\cdot(E+\omega)\cdot(E+3\omega)}\\ &\cdot[p_\perp\cdot J_{n-2}(\zeta_{\rm l},\frac{-z}{2})\cdot J_n(\zeta_{\rm l},\frac{-z}{2})]/\{[Z^2\\ &+((n-z)\boldsymbol{k}-\boldsymbol{p})^2]^2\cdot[Z^2+((n-2-z)\boldsymbol{k}-\boldsymbol{p})^2]^2\}\\ &+\sum_{n\geqslant n_0-1}\frac{128(n-z)^2\omega^2Z^5}{(\frac{\sqrt{I}}{\omega^2})^2\cdot(E+3\omega)^2}\\ &\cdot\frac{|J_{n-2}(\zeta_{\rm l},\frac{-z}{2})|^2\cdot p_\perp}{[Z^2+((n-2-z)\boldsymbol{k}-\boldsymbol{p})^2]^4}.\end{aligned} \tag{21}$$

The ionization rate per unit of longitudinal momentum for the excited state is investigated, illustrating

the obvious difference between the excited state and the ground state, considering that the initial bound electron will differ in the orientation associated with the angular momentum when the laser field propagates along the z-axis.[28] On the other hand, a similar result will be obtained even if the initial bound electron rotates in the opposite direction. The ionization rate per unit of longitudinal momentum of the outgoing electron from the excited state of a hydrogen atom can be written as

$$\begin{aligned}\frac{dW_1'}{dp_z} = \int d\varphi \sum_{n\geqslant n_0} & \frac{2p_\perp^3(n-z)^2\omega^2(Z/2)^7|J_n(\zeta_1,\frac{-z}{2})|^2}{[(Z/2)^2+((n-z)\boldsymbol{k}-\boldsymbol{p})^2]^6} \\ & + \sum_{n\geqslant n_0-1} \frac{8p_\perp^3(n-z)^2\omega^2(Z/2)^7}{(\sqrt{I}/\omega^2)^2\cdot(E+\omega)^2} \\ & \cdot \frac{|J_n(\zeta_1,\frac{-z}{2})|^2}{[(Z/2)^2+((n-z)\boldsymbol{k}-\boldsymbol{p})^2]^6} \\ & + \sum_{n\geqslant n_0-1} \frac{16p_\perp^3(n-z)^2\omega^2(Z/2)^7}{(\sqrt{I}/\omega^2)^2\cdot(E+\omega)\cdot(E+3\omega)} \\ & \cdot [J_n(\zeta_1,\frac{-z}{2})J_{n-2}(\zeta_1,\frac{-z}{2})]/\{[(Z/2)^2 \\ & + ((n-z)\boldsymbol{k}-\boldsymbol{p})^2]^3[(Z/2)^2 \\ & + ((n-2-z)\boldsymbol{k}-\boldsymbol{p})^2]^3\} \\ & + \sum_{n\geqslant n_0-1} \frac{8p_\perp^3(n-z)^2\omega^2(Z/2)^7}{(\sqrt{I}/\omega^2)^2\cdot(E+3\omega)^2} \\ & \cdot \frac{1}{[(Z/2)^2+((n-2-z)\boldsymbol{k}-\boldsymbol{p})^2]^6}. \end{aligned} \tag{22}$$

Observing Eqs. (21) and (22), the linear momentum relation modified through $\int d^3\boldsymbol{p}'\tilde{\phi}_{\rm i}(\boldsymbol{p}')\cdot\delta(\boldsymbol{p}'-\boldsymbol{p}+(n-z)\cdot\boldsymbol{k}) = \tilde{\phi}_{\rm i}(\boldsymbol{p}+(z-n)\cdot\boldsymbol{k})$ directly contributes to the numerical result of the PLMD. The important relation is responsible for the asymmetry structure associated with the correction dipole approximation. The numerical value of the PLMD will increase, in sharp contrast with that calculated under dipole approximation, when the direction of the ejected electron longitudinal momentum is parallel to the laser beam and vice versa. Figures 1 and 2 reveal that the peak shifts along the positive axis when the ground and excited states respectively are adopted as the initial state. Figures 1 and 2 show the same conditions as in Ref. [14] for the laser at 3400 nm and 0.06 PW. The peak of the structure in Fig. 1 is located at $p_z \cong 3.7\times10^{-3}$ a.u.$\cong 38|\boldsymbol{k}|$, whereas that in Fig. 2 can be found at $p_z \cong 0.001$ a.u.$\cong 10|\boldsymbol{k}|$. Two terms (i.e., $[Z^2+((n-2-z)\boldsymbol{k}-\boldsymbol{p})^2]^{-4}$ and $[(Z/2)^2+((n-2-z)\boldsymbol{k}-\boldsymbol{p})^2]^{-6}$) are adopted to account for the issue in Eqs. (21) and (22), respectively, by denoting the linear momentum relation. The shift tendency is more apparent for the electron from the ground state of a hydrogen atom than the electron from the excited state of a hydrogen atom since the photoelectrons released from the ground absorb more photos to be liberated, which brings about more apparent asymmetry in PLMD. These results are analogous to those presented in Fig. 5(b) in Ref. [16], which indicates the positive shifts of the whole p_z distribution are related to the Lorentz force. Here $\boldsymbol{B} = \nabla\times\boldsymbol{A}$[21] responds to the characteristic phenomenon observed when the vector potential is employed, which is described by completing the electric and magnetic fields with the $\omega t-\boldsymbol{k}\cdot\boldsymbol{r}$ phase dependence.

$$\begin{aligned}\frac{dW_c}{dp_z} = \int d\varphi\Big\{ & \sum_{n\geqslant n_0} \frac{32(n-z)^2\omega^2Z^5p_\perp|J_n(\xi_c)|^2}{[Z^2+((n-z)\boldsymbol{k}-\boldsymbol{p})^2]^4} \\ & - \frac{64(n-z)^2\omega^2Z^5p_\perp|J_n(\xi_c)|^2}{(\sqrt{I/2}\cdot E/\omega^2)^2\cdot[Z^2+(((n-z)\boldsymbol{k}-\boldsymbol{p})^2)]^4}\Big\}. \end{aligned} \tag{23}$$

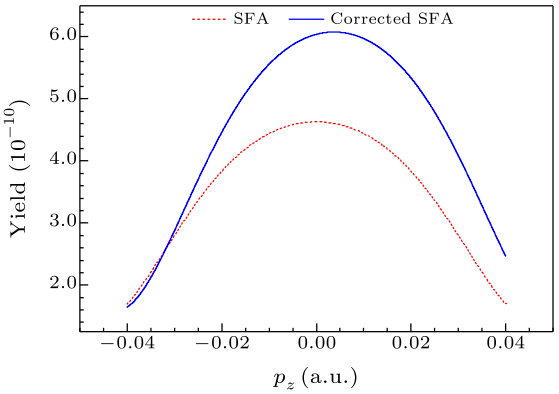

Fig. 1. Photoelectron momentum spectra of the ground state produced by linearly polarized laser at intensity 60 TW/cm^2 and wavelength 3.4 μm. The red line represents the spectra calculated by SFA, and the blue line shows the spectra with correction. The cusp is moved by 0.0037 a.u. due to the considered correction.

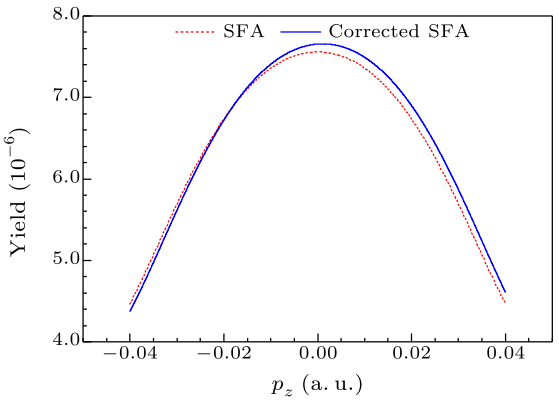

Fig. 2. Photoelectron momentum spectra of excited state produced by linearly polarized laser at intensity 60 TW/cm^2 and wavelength 3.4 μm. The red line represents the spectra calculated by SFA, and the blue line shows the spectra with correction. The peak is shifted approximately by 0.001 a.u. due to the considered correction, which is less obvious compared with the ground state of hydrogen.

Similarly, we calculate the PLMD produced by the circularly polarized laser at 1400 nm and 0.8 PW according to Eq. (23), which represents the ionization rate per unit of longitudinal momentum. Figure 3 shows the peak shifts along the beam propagation direction. The key factor, which is the breakdown of the dipole approximation, is introduced to explain the ionization produced by the circularly polarized laser

and the direct ionization produced by the linearly polarized laser. From the comparison of photoelectrons liberated from atoms by the linearly polarized laser, the peak offset is obviously shifted in the PLMD when the ionization is caused by circularly polarized lasers. On the other hand, the peak offset is increased with the intensities of laser, as shown in Fig. 4.

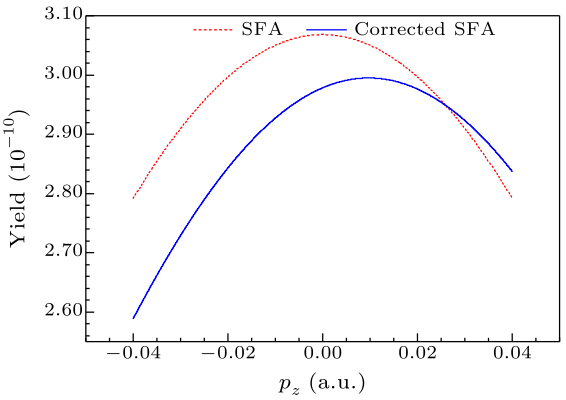

Fig. 3. Photoelectron momentum spectra of ground state produced by circularly polarized laser at 1400 nm and 0.8 PW. The red line represents the spectra calculated by SFA, and the blue line shows the spectra with correction. The peak is shifted by 0.0097 a.u. due to the considered correction roughly, which is analogous with the results reported in Ref. [9].

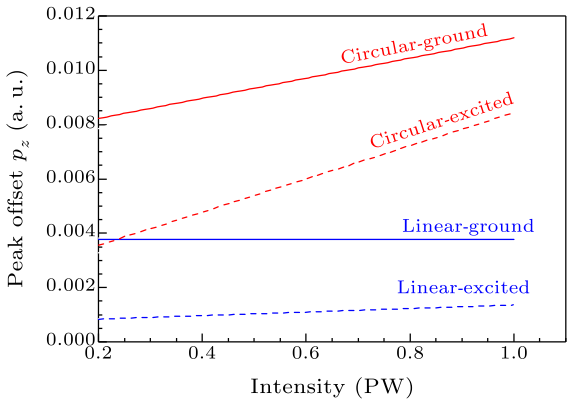

Fig. 4. The intensity dependence of the center of distribution is exhibited for ionization in 1400 nm when linearly polarized lasers and circularly polarized laser, respectively, stimulate photoelectrons. The PLMD are shown when the photoelectrons come from different initial states.

This discussion ensures that the asymmetry along the beam propagation direction can be explained by introducing the correction of the dipole approximation. Meanwhile, the re-scattering process[16,29,30] is responsible for the shift in the peak of this projection in the direction opposite to the beam propagation direction, including that with the laser of short wavelength.[30] We have emphasized here the importance and meaning of the influence exerted by the breakdown of the dipole approximation in the direct ionization, calculated through the SFA theory.

In conclusion, a new approach for analyzing the direct PLMD has been raised based on the SFA theory. The validity of the decrease in dipole approximation has been demonstrated in the tunnel ionization due to enormously strong intensity and extremely low frequency, which directly causes the asymmetry of the PLMD. Regardless of the ionization produced by the linearly or circularly polarized laser, a positive shift in peak can be observed in the PLMD because of the nondipole effects when the direct ionization happens. On the other hand, for the photoelectron released from the hydrogen-like atom ionized via the circularly polarized laser, the peak is shifted more apparently than the photoelectron released by linearly polarized laser. When the photoelectron is released from the ground state of the hydrogen-like atom, the characteristic peak offset can be obviously observed. Moreover, the peak offset in PLMD is increased with the intensities of laser. It is reasonable that the outgoing electron is initially pushed in the beam propagation direction. Conversely, some photoelectrons can be deflected by the parent ion.[16]

References

[1] Keldysh L V 1965 *Sov. Phys. JETP* **20** 1307
[2] Reiss H 1980 *Phys. Rev.* A **22** 1786
[3] Faisal F H M 1973 *J. Phys.* B **6** L89
[4] Wu M Y et al 2013 *Chin. Phys. Lett.* **30** 073202
[5] Hao X L et al 2012 *Chin. Phys.* B **21** 083304
[6] Weber Th et al 2000 *Phys. Rev. Lett.* **84** 443
[7] Chen J and Nam C H 2002 *Phys. Rev.* A **66** 053415
[8] Chen Z et al 2006 *Phys. Rev.* A **74** 053405
[9] Ivanov I A 2014 *Phys. Rev.* A **90** 013418
[10] Arissian L et al 2010 *Phys. Rev. Lett.* **105** 133002
[11] Smeenk C T L et al 2011 *Phys. Rev. Lett.* **106** 193002
[12] Titi A S and Drake G W 2012 *Phys. Rev.* A **85** 041404
[13] Reiss H R 2013 *Phys. Rev.* A **87** 033421
[14] Ludwig A et al 2014 *Phys. Rev. Lett.* **113** 243001
[15] Corkum P B 1993 *Phys. Rev. Lett.* **71** 1994
[16] Chelkowski S et al 2015 *Phys. Rev.* A **92** 051401(R)
[17] Blaga C I et al 2009 *Nat. Phys.* **5** 335
[18] Wu C Y et al 2012 *Phys. Rev. Lett.* **109** 043001
[19] Reiss H R 2008 *Phys. Rev. Lett.* **101** 043002
[20] Reiss H R 2014 *J. Phys.* B **47** 204006
[21] Reiss H R 2000 *Phys. Rev.* A **63** 013409
[22] Henneberge W C 1968 *Phys. Rev. Lett.* **21** 838(R)
[23] Gordon W 1926 *Z. Phys.* **40** 117
[24] Volkov D M 1935 *Z. Phys.* **94** 250
[25] Bauer J 2005 *Phys. Rev.* A **71** 067401
[26] Mishima K et al 2002 *Phys. Rev.* A **66** 053408
[27] Salamin Y I 1997 *Phys. Rev.* A **56** 4910
[28] Bauer J 2013 *J. Phys.* B **46** 045601
[29] Tao J F et al 2017 *Phys. Rev.* A **95** 011402(R)
[30] Chelkowski S et al 2017 *Phys. Rev.* A **95** 053402